Inhibition of BCL2 Family Members Increases the Efficacy of Copper Chelation in BRAF^{V600E}-Driven Melanoma

Ye-Jin Kim[1], Tiffany Tsang[2], Gray R. Anderson[3], Jessica M. Posimo[1], and Donita C. Brady[1,4]

ABSTRACT

The principal unmet need in BRAF^{V600E}-positive melanoma is lack of an adequate therapeutic strategy capable of overcoming resistance to clinically approved targeted therapies against oncogenic BRAF and/or the downstream MEK1/2 kinases. We previously discovered that copper (Cu) is required for MEK1 and MEK2 activity through a direct Cu–MEK1/2 interaction. Repurposing the clinical Cu chelator tetrathiomolybdate (TTM) is supported by efficacy in BRAF^{V600E}-driven melanoma models, due in part to inhibition of MEK1/2 kinase activity. However, the antineoplastic activity of Cu chelators is cytostatic. Here, we performed high-throughput small-molecule screens to identify bioactive compounds that synergize with TTM in BRAF^{V600E}-driven melanoma cells. Genetic perturbation or pharmacologic inhibition of specific members of the BCL2 family of antiapoptotic proteins (BCL-W, BCL-XL, and MCL1) selectively reduced cell viability when combined with a Cu chelator and induced CASPASE-dependent cell death. Further, in BRAF^{V600E}-positive melanoma cells evolved to be resistant to BRAF and/or MEK1/2 inhibitors, combined treatment with TTM and the clinically evaluated BCL2 inhibitor, ABT-263, restored tumor growth suppression and induced apoptosis. These findings further support Cu chelation as a therapeutic strategy to target oncogene-dependent tumor cell growth and survival by enhancing Cu chelator efficacy with chemical inducers of apoptosis, especially in the context of refractory or relapsed BRAF^{V600E}-driven melanoma.

Significance: This study unveils a novel collateral drug sensitivity elicited by combining copper chelators and BH3 mimetics for treatment of BRAF^{V600E} mutation-positive melanoma.

Introduction

Melanoma is driven in 40% to 50% of cases by activating mutations in the *BRAF* serine/threonine kinases (1, 2). Over 90% of oncogenic BRAF mutations detected in melanoma are Val 600→Glu (V600E; refs. 3, 4). Activated BRAF^{V600E} phosphorylates and activates MEK1/2, which subsequently phosphorylate and activate ERK1/2, resulting in hyperactivation of the evolutionarily conserved MAPK pathway to drive melanomagenesis (4, 5). Thus, patients with late-stage BRAF^{V600E}-positive melanoma are typically treated with the FDA-approved combination of mutant-selective, ATP-competitive BRAF inhibitors (BRAFi, dabrafenib, and vemurafenib) and allosteric MEK1/2 inhibitors (MEK1/2i, trametinib, and cobimetinib; refs. 6–9). Although this standard of care is initially effective, patients with BRAF^{V600E}-mutant melanoma have only modest improvements in median progression-free survival and eventually develop resistance (4, 10, 11). The limited clinical durability of the combination has bolstered research aimed at additional combination strategies to forestall resistance development, targeting multiple signaling pathways capable of driving resistance, or exploring alternative pharmacologic accessible nodes within the MAPK pathway (4, 10, 11).

In search of identifying novel components of the canonical MAPK pathway, several groups have employed functional genomics approaches (12). Specifically, a whole-genome RNAi screen revealed that the primary copper (Cu) transporter *Ctr1* reduced ERK1/2 phosphorylation when knocked down in *Drosophila* S2 cells (13). We demonstrated that Cu directly binds to MEK1/2 and influences the strength of the RAF-MEK-ERK cascade (14). Leveraging the dependence of *BRAF* mutation–positive cancers on MEK1/2 for tumorigenesis (15), we found that decreasing the levels of *CTR1* or introducing surface accessible mutations in MEK1 that disrupt Cu binding decreased BRAF^{V600E}-driven signaling and tumor growth (16). Importantly, the Cu-selective chelator tetrathiomolybdate (TTM), used as an investigational treatment of Wilson disease (17), diminished tumorigenesis in models of BRAF^{V600E} melanoma (18). Although TTM use has not been clinically explored in BRAF^{V600E}-driven melanoma, TTM has been assessed in breast cancers as an antiangiogenic compound where patients have been treated safely for upwards of 65 months (19). Further, the combination of TTM, a well-tolerated and affordable drug, and vemurafenib led to a survival benefit in a murine model of metastatic melanoma, but failed to yield tumor regression (18).

In this study, we aimed to advance the therapeutic value of Cu chelation in BRAF^{V600E} melanomas by identifying compounds that enhanced TTM efficacy. We performed high-throughput small-molecule screens with a panel of bioactive compounds to explore collateral drug sensitivities in combination with TTM. Here, we demonstrate that cotargeting select BCL2 proteins via BH3 mimetics synergizes with Cu chelators in both naïve and resistant forms of BRAF^{V600E} melanoma cells. The findings presented here highlight the potential of inducing apoptosis and melanoma tumor suppression when Cu chelators are combined with BCL2is.

Materials and Methods

Reagents

A1210477 (ApexBio, B6011), ABT-199 (Selleck Chemicals, S8048), ABT-263 (M1637, AbMole), ABT-737 (Selleck Chemicals, S1002),

[1]Department of Cancer Biology, Perelman School of Medicine, University of Pennsylvania, Philadelphia, Pennsylvania. [2]Cell and Molecular Biology Graduate Group, Perelman School of Medicine, University of Pennsylvania, Philadelphia, Pennsylvania. [3]Department of Pharmacology and Cancer Biology, Duke University Medical Center, Durham, North Carolina. [4]Abramson Family Cancer Research Institute, Perelman School of Medicine, University of Pennsylvania, Philadelphia, Pennsylvania.

Note: Supplementary data for this article are available at Cancer Research Online (http://cancerres.aacrjournals.org/).

Corresponding Author: Donita C. Brady, Department of Cancer Biology, University of Pennsylvania, 421 Curie Blvd., 612 BRBII/II, Philadelphia, PA 19104. Phone: 215-573-9705; E-mail: bradyd@pennmedicine.upenn.edu

Cancer Res 2020;80:1387–400

doi: 10.1158/0008-5472.CAN-19-1784

Ammonium TTM (Sigma-Aldrich, 323446), trametinib (Selleck Chemicals, S2673), WEHI-539 hydrochloride (ApexBio, A8634), vemurafenib (CT-P4032), and Z-DEVD-FMK (Selleck Chemicals, S7312) were purchased from indicated companies.

Cell lines

293T/17 (ATCC, catalog #CRL-11268), A375 (ATCC, catalog #CRL-1619), WM88 (Rockland, catalog #WM88-01-0001), WM3311 (Rockland, catalog #WM3311-01-0001), and WM3743 (Rockland, catalog #WM3743-01-0001) cells were purchased from the indicated companies and maintained in DMEM (Gibco) supplemented with 10% v/v FBS (GE Lifesciences) and 1% penicillin–streptomycin (Gibco). 451Lu parental cells and resistant derivatives, 451-Lu BRAFi^R and 451-Lu MEKi^R, were a kind gift from Jessie Villanueva (Wistar Institute, Philadelphia, PA) and maintained in DMEM supplemented with 5 % FBS with 1 μmol/L vemurafenib or 1 μmol/L trametinib (20, 21). WM983B parental cells and a resistant derivative, WM983B BRAFi^R, were a kind gift from Jessie Villanueva (Wistar Institute) and maintained in DMEM supplemented with 5 % FBS with 1 μmol/L vemurafenib. Cell lines were not authenticated. Mycoalert testing was done to test for mycoplasma contamination of all cell lines. Derived cell lines were generated by stable infection with lentiviruses derived from the pSMARTvector-inducible lentiviral shRNA plasmids (Dharmacon, see plasmids below) or retroviruses derived from the pBABE retroviral plasmid (see plasmids below) described below using established methods.

Plasmids

pSMARTvector-inducible lentiviral shRNA plasmids were purchased from Dharmacon to express: nontargeted control, human BCL2 target sequence #1 5′-TGACGCTCTCCACACACAT, human BCL2 target sequence #2 5′-AAGAAGGCCACAATCCTCC, human BCL-XL target sequence #1 5′-CAAACTGCTGCTGTGGCCA, human BCL-XL target sequence #2 5′-CTCCGATTCAGTCCCTTCT, human BCL-W target sequence #1 5′-AGCGGGTCTCGAACTCATC, human BCL-W target sequence #2 5′-CTGCTGTGGATCCAGTCAG, human MCL1 target sequence #1 5′-CGAAGGAAGTATCGAATTT, human MCL1 target sequence #2 5′-AGAGTGTATACAGAACGAA. GFP and shRNA expression was induced by adding 0.5 μg/mL (for A375) or 1 μg/mL (for WM88) of doxycycline hydrochloride (Dox, Fisher Scientific, AAJ67043AE) to DMEM supplemented with 10% FBS and 1% penicillin–streptomycin, Gibco. pBABEpuro-HA-p61BRAF^{V600E}, pBABEpuro-HA-MEK1^{C121S}, and pBABEpuro-HA-PDGFRß were previously described (18).

Cell viability assay

Note that 5×10^3 of the indicated cells per well were plated in white 96-well plates (Fisher Scientific, 655098) and cultured for 12 hours prior to treatment with the indicated drugs for 72 or 96 hours. Cell viability was measured using CellTiter-Glo cell viability assay (Promega, G7571). Normalized %ATP values were calculated by normalizing luminescence values for each drug treatment condition to vehicle (DMSO)-treated wells. To generate IC_{50} curves, the nonlinear fit of Log(Drug) or Drug versus normalized response (%ATP Normalized to DMSO) with a variable slope was calculated in Prism8 (GraphPad). Each drug treatment condition was represented by at least three biological replicates plated in technical triplicate. The Bliss Index to test for synergy in drug combinations was performed as previously described (18, 22).

Flow cytometry

Note that 2×10^5 of the indicated cells were seeded in 6-well plates (Genesee Scientific, 25-105) and treated as described, floating and attached cells were harvested, and stained with Annexin V-FITC and propidium iodide (PI) using Annexin V-FITC apoptosis detection kit I (BD Biosciences, 556547) according to the manufacturer's protocols. Data were acquired using the Attune NxT flow cytometry (Thermo Scientific) and analyzed with FlowJo 8.7 (Tree Star).

Immunoblot analysis

Indicated cells or xenograft-derived tumor lysates were treated as indicated and then washed with cold 1X PBS and lysed with cold RIPA buffer containing 1X EDTA-free Halt protease and phosphatase inhibitor cocktail (Thermo Scientific, 78441). The protein concentration was determined by BCA Protein Assay (Pierce) using BSA as a standard. Equal amounts of lysates were resolved by SDS-PAGE using standard techniques, and protein was detected with the following primary antibodies: rabbit anti-phospho (Thr202/Tyr204)-ERK1/2 [1:1,000; Cell Signaling Technology (CST), 9101], mouse anti-ERK1/2 (1:1,000; CST, 9107), rabbit anti-phospho (Ser217/221)-MEK1/2 (1:1,000; CST, 9154), mouse anti-MEK1/2 (1:1,000; CST, 4694), rabbit anti-PARP (1:1,000; CST, 9542), rabbit anticleaved PARP (1:1,000; CST, 9541), rabbit anti-CASPASE-3 (1:1,000; CST, 9662), mouse anti–β-actin (1:10,000; CST, 3700), rabbit anti-BCL2 (1:1,000; CST, 4223), rabbit anti–BCL-W (1:1,000; CST, 2724), rabbit anti–BCL-XL (1:1,000; CST, 2764), rabbit anti–MCL1 (1:1,000; CST, 94296), rabbit anti-CYTOCHROME C (1:1,000; CST 11940), rabbit anti-HSP60 (1:1,000; CST 4870), mouse anti–α-TUBULIN (1:1,000; CST 3873), followed by detection with one of the horseradish peroxidase–conjugated secondary antibodies: goat anti-rabbit IgG (1:5,000; CST, 7074) or goat anti-mouse IgG (1:5,000; CST, 7076), using SignalFire (CST) or SignalFire Elite ECL (CST) detection reagents. For detection of CYTOCHROME-C release, cells were treated as described, washed with cold 1X PBS, and mitochondrial and cytosolic fractions were separated using mitochondria/cytosol fractionation kit (BioVision K256) according to the manufacturer's protocols.

High-throughput small-molecule library screen

Drug screening was performed by the University of Pennsylvania High-Throughput Screening Core. To determine the IC_{20} for the indicated cell lines, 10^3 cells were plated per well in white 384-well plates, treated with eight concentrations of TTM (1:3 dilution, ranging from 0.0457 to 100 μmol/L), and cell viability was measured 96 hours later with the ATPlite cell viability assay (Perkin Elmer) on an EnVision Plate Reader (Perkin Elmer). To generate IC_{50} curves, the logistic regression curve of Log(Drug) versus normalized response (%ATP Normalized to DMSO) was fit in TIBCO Spotfire software. The IC_{20} was calculated using the following formula: IC_F = [(F/(100-F)^(1/H)]*IC_{50}, where H = the Hill slope. For the subsequent drug screens, indicated cell lines were treated with 100 nmol/L of a compound from the SelleckChem Bioactive Compound Library with or without TTM at the IC_{20} for the respective cell line. DMSO and doxycycline were used as negative and positive controls, respectively. Normalized percent inhibition (NPI) was calculated for all data points.

Mouse xenografts and drug treatments

All studies were approved by the University of Pennsylvania Institutional Animal Care and Use Committee. Note that 5×10^6 A375,451-Lu-BRAFi^R, or 451-Lu-MEKi^R or 8×10^6 451-Lu cells resuspended in 1X PBS were injected s.c. into flanks of SCID/beige

mice (Charles River Laboratory) as previously described (23). When tumor volume reached approximately 100 mm^3, mice were treated daily via oral gavage: vehicle [1% methylcellulose (Sigma-Aldrich, M0512), 1% DMSO (Sigma-Aldrich)]; 80 mg/kg TTM in vehicle; 25 mg/kg vemurafenib in 10% ethanol, 30% polyethylene glycol (PEG) 400 (EMD Millipore, 8.07485.1000), and 60% Phosal 50PG (Lipoid, 368315); 0.5 mg/kg trametinib in PEG; or 25 mg/kg ABT-263 in PEG.

Immunofluorescence

Tumor tissue sections were stained with either a rabbit anti-Ki67 antibody (1:100; Novus Biologicals, NB100-89717) followed by detection with a Alexa Fluor 647–conjugated anti-rabbit IgG (1:1,000; Thermo Scientific, A27040) or DeadEnd Colorimetric TUNEL System (Promega, G3250), following the manufacturer's protocol. Photographs were taken on a Leica DMI6000B–inverted confocal microscope (40x) in a blinded fashion. Images were quantified using Image J software.

Results

TTM-mediated reductions in BRAF^{V600E}-driven cell viability and MAPK signaling fail to induce apoptosis

To examine whether Cu chelator efficacy could be improved in BRAF^{V600E}-positive melanoma, we first treated BRAF^{V600E}-mutant melanoma cells *in vitro* with increasing concentrations of TTM and measured cell viability. TTM reduced the number of viable 451-Lu, A375, WM88, and WM983B cells in a dose-dependent manner (**Fig. 1A–E**). However, TTM treatment failed to increase the percentage of apoptotic cells (**Fig. 1F–I**), as measured by Annexin V and PI positivity via flow cytometry (24), despite effectively decreasing ERK1/2 phosphorylation (**Fig. 1J–M**; Supplementary Fig. S1A–S1D). In agreement, cleavage of CASPASE-3 and PARP (25, 26), well-known markers of cells undergoing apoptosis, were only observed at concentrations higher than the IC_{50} of TTM (**Fig. 1J–M**; Supplementary Fig. S1A–S1D). Similarly, treatment with either MAPKi (Supplementary Fig. S2A–S2J) was not sufficient to increase markers of apoptosis (Supplementary Fig. S2K–S2R). Thus, *in vitro* Cu chelators blunt MAPK pathway activation and inhibit the viability of BRAF^{V600E}-driven melanoma cells but fail to induce apoptosis, akin to treatment with MAPKis, and support the rationale to identify other therapeutic combinations to improve Cu chelation therapy.

BH3 mimetics synergize with TTM to reduce cell viability of BRAF^{V600E}-driven melanoma cells

In order to identify collateral drug sensitivities with Cu chelators, we investigated combination of a minimally inhibitory dose of TTM with the Selleckchem bioactive compound library composed of a unique collection of 2123 bioactive chemical compounds, which are either FDA-approved or have known bioactivity and safety profiles (**Fig. 2A**). A375 and WM88 cells were treated with a low dose of each individual compound within the Selleckchem bioactive compound library and either vehicle or the respective IC_{20} of TTM (**Fig. 2A**). A 20% reduction in A375 and WM88 cell viability was achieved for the majority of the bioactive compounds, which reflected TTM efficacy alone, and indicated that most of the bioactive compounds displayed minimal efficacy alone at 100 nmol/L (Supplementary Fig. S3A and S3B). Therefore, initial hits were restricted to compounds that when combined with TTM yielded the intended 20% or greater inhibition of cell viability (**Fig. 2B** and **C**; Supplementary Fig. S3A and S3B). Further, synergistic combinations with TTM were identified by calculating the Bliss Index (22), which considers the expected additive effect of a drug combination compared with the observed effect, for each initial compound hit (NPI TTM + Compound ≥20; **Fig. 2D** and **E**). Fifty and 233 bioactive compounds synergistically inhibited cell viability of A375 or WM88 cells, respectively, with a Bliss Index ≥1.5 (**Fig. 2F** and **G**). Only five bioactive compounds scored as hits (NPI TTM + Compound ≥20/Bliss Index ≥1.5) in both BRAF^{V600E}-positive melanoma cells (**Fig. 2H** and **I**). These findings establish the utility of employing high-throughput small-molecule screens to identify synergistic drug combinations for potential cancer treatment and more importantly suggest that several bioactive compounds may be useful to enhance Cu chelation therapy efficacy in BRAF^{V600E}-mutant melanoma.

We were keenly interested in our finding that the pan BH3 mimetic ABT-737 synergistically inhibited the viability of both A375 and WM88 cells to the greatest extent when combined with TTM (**Fig. 2I**). The B-cell lymphoma-2 (BCL2) family consists of two types of proteins (27), antiapoptotic (e.g., BCL2, BCL-XL, BCL-W, and MCL1; refs. 28–30) and proapoptotic (e.g., BAK, BAX, and BIM), which cooperate through homo- or heterodimer formation to retain the balance between cell survival and death (31–33). Drugs termed "BH3 mimetics" that bind the surface groove of certain antiapoptotic BCL2 proteins and thereby elicit apoptosis have been developed (34–40). Among them, successful clinical trials of venetoclax (ABT-199), a specific BCL2i, has led to its FDA approval for chronic lymphocytic leukemia and clinical evaluation for treatment of other cancers (41–44). However, single-agent inhibition of BCL2 is not sufficient to induce cell death of melanomas due in part to differential BCL2 protein expression and diversity (45–51). Similarly, ABT-199 failed to significantly reduce *BRAF*-mutant melanoma cell viability alone or in combination with TTM in the high-throughput screen (Supplementary Fig. S3C). Inhibition of multiple antiapoptotic BCL2 proteins is a major target for melanoma and other cancers (34, 46).

Collateral inhibition of oncogenic MAPK signaling and BCL2 proteins with the pan-BH3 mimetic, ABT-737, reduces targeted therapy resistance in BRAF^{V600E}-driven melanoma (52–54). In support of these findings, combining MAPKis and navitoclax (ABT-263), an orally bioavailable analog of ABT-737 (NCT01989585), is being tested clinically in BRAF^{V600E}-positive melanoma. Although not every BH3 mimetic in the high-throughput screen increased the efficacy of TTM, ABT-263 synergistically reduced A375 cell viability but was only additive in the WM88 cell line (Supplementary Fig. S3C). Combination of IC_{20} or IC_{50} doses of TTM and 100 nmol/L ABT-737 was sufficient to significantly reduce cell viability (**Fig. 2J** and **K**), but failed to increase the percentage of Annexin V–positive cells, cleaved-CASPASE-3, or cleaved-PARP (Supplementary Fig. S3D–S3G). Further, the addition of TTM to the combination of vemurafenib and ABT-737 or trametinib and ABT-737 significantly reduced A375 and WM88 cell viability (**Fig. 2L–O**). Treatment with TTM, ABT-737, and either MAPKi was either equivalent or superior to the combination of vemurafenib, trametinib, and ABT-737 (**Fig. 2L–O**). Finally, TTM significantly increased the capacity of the combination of the MAPKis and ABT-737 to reduce A375 cell viability (**Fig. 2L**). These findings indicate that Cu chelation therapy may be a viable alternative to either MAPKi when combined with a BH3 mimetic and, more importantly, could enhance the therapeutic benefit of the clinically investigated combination of the MAPKis and a BH3 mimetic.

Genetic loss of select antiapoptotic BCL2 family proteins decreases TTM IC_{50} in BRAF^{V600E}-driven melanoma cells

We next explored what molecular target(s) of ABT-737 impart(s) sensitivity to Cu chelators. ABT-737 selectively targets the

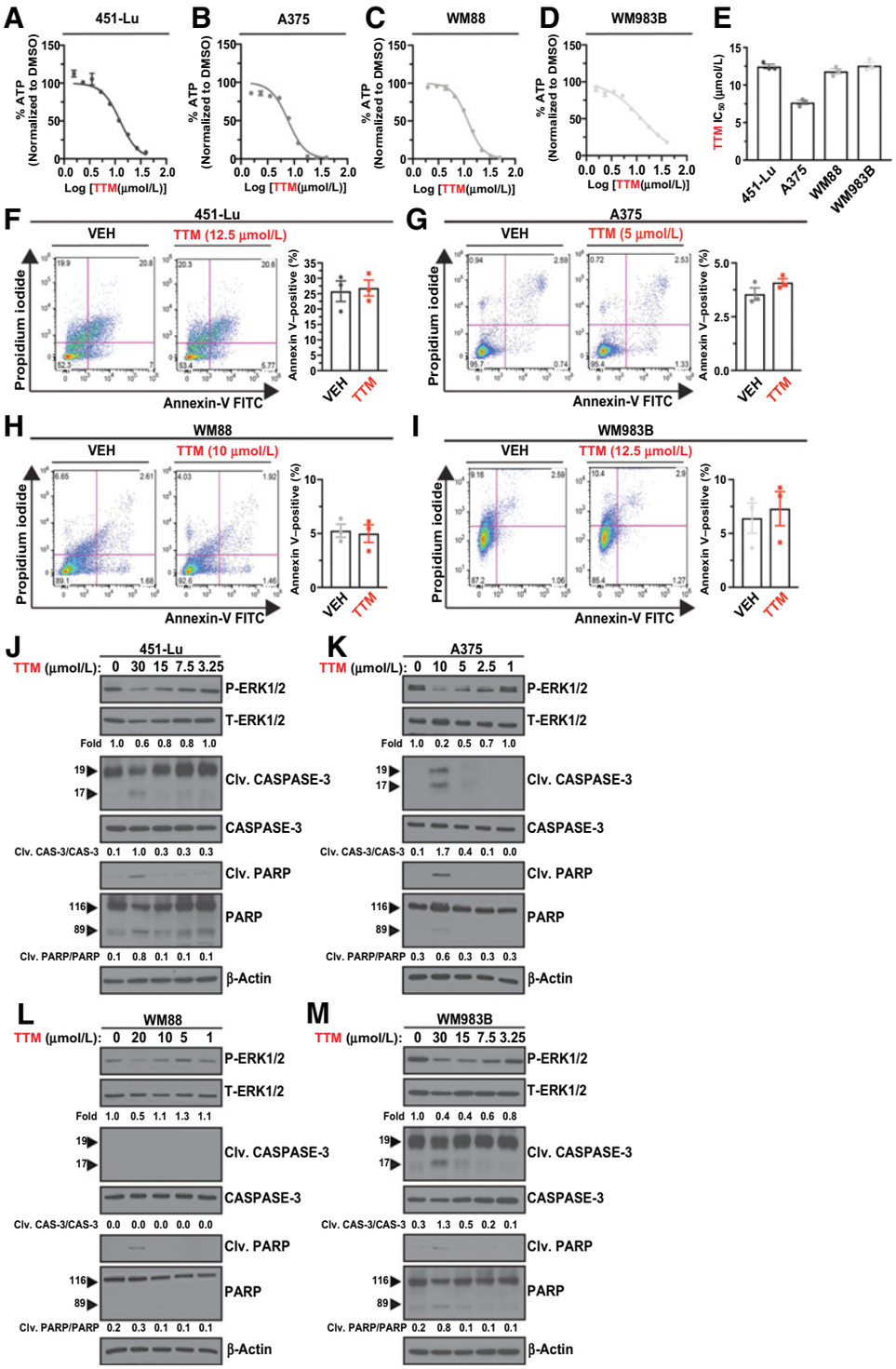

Figure 1.

TTM reduces MAPK pathway activation and viability without inducing apoptosis in $BRAF^{V600E}$-positive melanoma cells. **A–D,** Relative CellTiter-Glo cell viability ± SEM of indicated cells treated with indicated concentrations of TTM. $n = 3$. **E,** Scatter dot plot of TTM IC_{50} in indicated cell lines ± SEM. **F–I,** Representative flow cytometry graphs and scatter dot plots of flow cytometry analysis of Annexin V-FITC and PI ± SEM from indicated cell lines treated with vehicle (VEH) or TTM. $n = 3$. **J–M,** Immunoblot detection of phosphorylated (P)-ERK1/2, total (T)-ERK1/2, Cleaved (Clv.) CASPASE-3, CASPASE-3, Clv. PARP, PARP, and β-actin from indicated cells treated with vehicle or TTM. $n = 3$. Quantification: P-ERK1/2/T-ERK1/2 normalized to vehicle control and fold change Clv. CASPASE-3/CASPASE-3 and Clv. PARP/PARP.

antiapoptotic proteins, BCL2, BCL-W, and BCL-XL, but not MCL1 or A1 (37). Knockdown of *BCL-XL, BCL-W*, or *MCL1* with two independent doxycycline-inducible shRNAs increased TTM effectiveness in both A375 and WM88 cells (Supplementary Fig. S4A and S4B), as measured by a statistically significant shift in the IC_{50} of TTM in the presence of doxycycline (**Fig. 3A–D**). In contrast, depletion of *BCL2* failed to decrease TTM IC_{50} (**Fig. 3A–D**). These results suggest that lowering the antiapoptotic balance of BRAF^{V600E}-mutant melanoma cells by targeting specific antiapoptotic BCL2 proteins, BCL-W, BCL-XL, or MCL1, can enhance Cu chelator efficacy.

TTM enhances efficacy of select BH3 mimetics and induces apoptosis in BRAF^{V600E}-driven melanoma cells

To further examine the generalizability of combining Cu chelators with BH3 mimetics in BRAF^{V600E} mutation–positive melanoma, we tested whether treatment with TTM could lower the IC_{50} of a panel of four BH3 mimetics, ABT-737 (37), ABT-199 (BCL2i; ref. 38), WEHI-539 (BCL-XLi; ref. 39), and A1210477 (MCL1i; ref. 40). ABT-737 IC_{50} was significantly decreased by approximately 3-fold in A375 cells and approximately 10-fold in WM88 cells when cotreated with the highest concentration of TTM (**Fig. 3E–H**). However, the *BRAF* mutation–negative melanoma cell lines, WM3311 and WM3743, did not show a similar dose dependence when TTM and ABT-737 were coadministered (Supplementary Fig. S4C and S4D), suggesting that BRAF^{V600E}-mutant melanomas are selectively sensitive to the combination. The efficacy of WEHI-539 and A1210477 was also substantially enhanced with TTM (**Fig. 3E–H**). TTM only slightly decreased the IC_{50} of ABT-199 in either A375 or WM88 cells (**Fig. 3E–H**). Further, combination of TTM with ABT-737, WEHI-539, or A1210477 synergistically inhibited A375 and WM88 cell viability, whereas combining TTM with ABT-199 was additive by Bliss Indexes (**Fig. 3I** and **J**). Collectively, the above results suggest that the combined effects of TTM and BH3 mimetics on *BRAF*-mutant melanoma cell viability are driven by targeting BCL-W, BCL-XL, and/or MCL1, but not BCL2.

Melanomas are known to harbor elevated levels of the antiapoptotic BCL2 proteins (55, 56), which underlies intrinsic resistance to BH3 mimetics. Mechanistically, treatment of *BRAF*-mutant melanoma cells with TTM was sufficient to selectively reduce ERK1/2 phosphorylation and the expression of at least two BCL2 proteins (**Fig. 4A** and **B**; Supplementary Fig. S5A and S5B). The differential expression of BCL-W, BCL-XL, and/or MCL1 correlated with significantly increased cytosolic CYTOCHROME-C in A375 or WM88 cells treated with both TTM and ABT-737 (**Fig. 4C** and **D**; Supplementary S5C and S5D), indicating that mitochondrial outer membrane permeabilization (MOMP) was triggered. In turn, cotreatment with TTM and ABT-737 increased the population of cells undergoing apoptotic cell death by 2- or 3-fold (**Fig. 4E** and **F**). Finally, cleaved CASPASE-3 and PARP levels, which are initiated by MOMP-mediated CYTOCHROME-C release, were elevated following cotreatment with TTM and any of the three BH3 mimetics, ABT-737, WEHI-539, and A1210477 (**Fig. 4G–J**; Supplementary Fig. S5E–S5G). As expected, preincubation of A375 or WM88 cells with the irreversible CASPASE-3i Z-DEVD-FMK blunted the induction of markers of apoptosis in response to the combination of TTM and ABT-737 (**Fig. 4E–H**; Supplementary Fig. S5E and S5F). Taken together, these results revealed that Cu chelation can enhance the apoptotic activity of BH3 mimetics in a CASPASE-dependent manner in BRAF^{V600E}-driven melanoma cells.

TTM treatment with ABT-737 sensitizes trametinib- or vemurafenib-resistant BRAF^{V600E}-positive melanoma cells

To interrogate the utility of combining Cu chelation with BH3 mimetics to restore apoptotic cell death in the setting of MAPKi acquired resistance, we employed BRAFi- or MEK1/2i-resistant variants of the BRAF^{V600E}-mutant cell lines 451-Lu and WM983B (20, 21). Treatment with TTM, trametinib, or vemurafenib reduced the IC_{50} of ABT-737 in parental 451-Lu and WM983B cells (**Fig. 5A** and **B**; Supplementary Fig. S6A and S6B). Whereas in 451-Lu-BRAFi^R and WM983B-BRAFi^R cells, both TTM and trametinib markedly decreased ABT-737 IC_{50} (**Fig. 5C** and **D**; Supplementary Fig. S6C and S6D), whereas only TTM was sufficient to sensitize the MEK1/2i-resistant 451-Lu cells to the BH3 mimetic (**Fig. 5E** and **F**). Further, cotreatment with TTM and ABT-737 was the only synergistic combination in both the parental and resistant cell lines based on Bliss Indexes (**Fig. 5G–I**; Supplementary Fig. S6E and S6F). As such, TTM treatment enhanced the efficacy of a BH3 mimetic in the setting of MAPKi resistance.

Combining the Cu chelator and BH3 mimetic in the clinically relevant setting of MAPKi resistance revealed that the combination was more efficacious than the FDA-approved combination of vemurafenib and trametinib in both the naïve and MAPKi-resistant 451-Lu and WM983B cells (**Fig. 5L–O**; Supplementary Fig. S6G–S6J). In addition, TTM significantly increased the efficacy of the MAPKis and BH3 mimetic in WM983B cells (Supplementary Fig. S6G and S6H). Most importantly, TTM treatment significantly improved the efficacy of ABT-737 combined with the MAPKis in each of the MAPKi-resistant *BRAF* mutation–positive melanoma cells (**Fig. 5L–O**; Supplementary Fig. S6I and S6J). Thus, Cu chelators may be advantageous in improving the response to the combination of a BRAFi, MEK1/2i, and BH3 mimetic being tested clinically and more importantly be an additional treatment option in the context of MAPKi resistance.

TTM dampens the apoptotic threshold in response to BH3 mimetics by limiting antiapoptotic protein expression in MAPKi-resistant BRAF^{V600E}-positive melanoma cells

Next, we tested and found in parental cells, MAPK signaling was abrogated by either TTM or MAPKi treatment, but unlike TTM that significantly decreased the expression of BCL-W, BCL-XL, and/or MCL1, trametinib failed to impact the levels of BCL2 proteins (**Fig. 6A**; Supplementary Fig. S7A). Interestingly, vemurafenib significantly decreased the expression of BCL2 and BCL-W in 451-Lu cells only (**Fig. 6A**; Supplementary Fig. S7A). Thus, surprisingly the pattern of BCL2 protein expression was divergent among the 451-Lu or WM983B cells treated with TTM or the MAPKis (**Fig. 6A**; Supplementary Fig. S7A–S7C). The BRAFi-resistant 451-Lu and WM983B cells (20, 21), which harbor upregulation of receptor tyrosine kinases as a resistance mechanism, and MEK1/2i-resistant 451Lu cells (20, 21), which harbor a Q60P-activating mutation in MEK2 and *BRAF* amplification as a resistance mechanism, displayed elevated MEK1/2 and ERK1/2 phosphorylation (**Fig. 6A–C**; Supplementary Fig. S7A–S7D). Increased MAPK signaling in the BRAFi-resistant variants was dampened by TTM and trametinib treatment but not the mutant selective BRAFi vemurafenib (**Fig. 6B**; Supplementary Fig. S7B–S7D). Of clinical relevance, TTM treatment of the dual MAPKi-resistant 451-Lu cells was sufficient to reduce ERK1/2 phosphorylation, along with BCL-W, BCL-XL, and MCL1 expression, which may explain the maintained sensitivity to the combination of TTM and ABT-737 in these cells (**Fig. 5C, E**, and **F**; Supplementary Fig. S7D). These findings indicate that the cooperativity between the Cu chelator and BH3 mimetic in

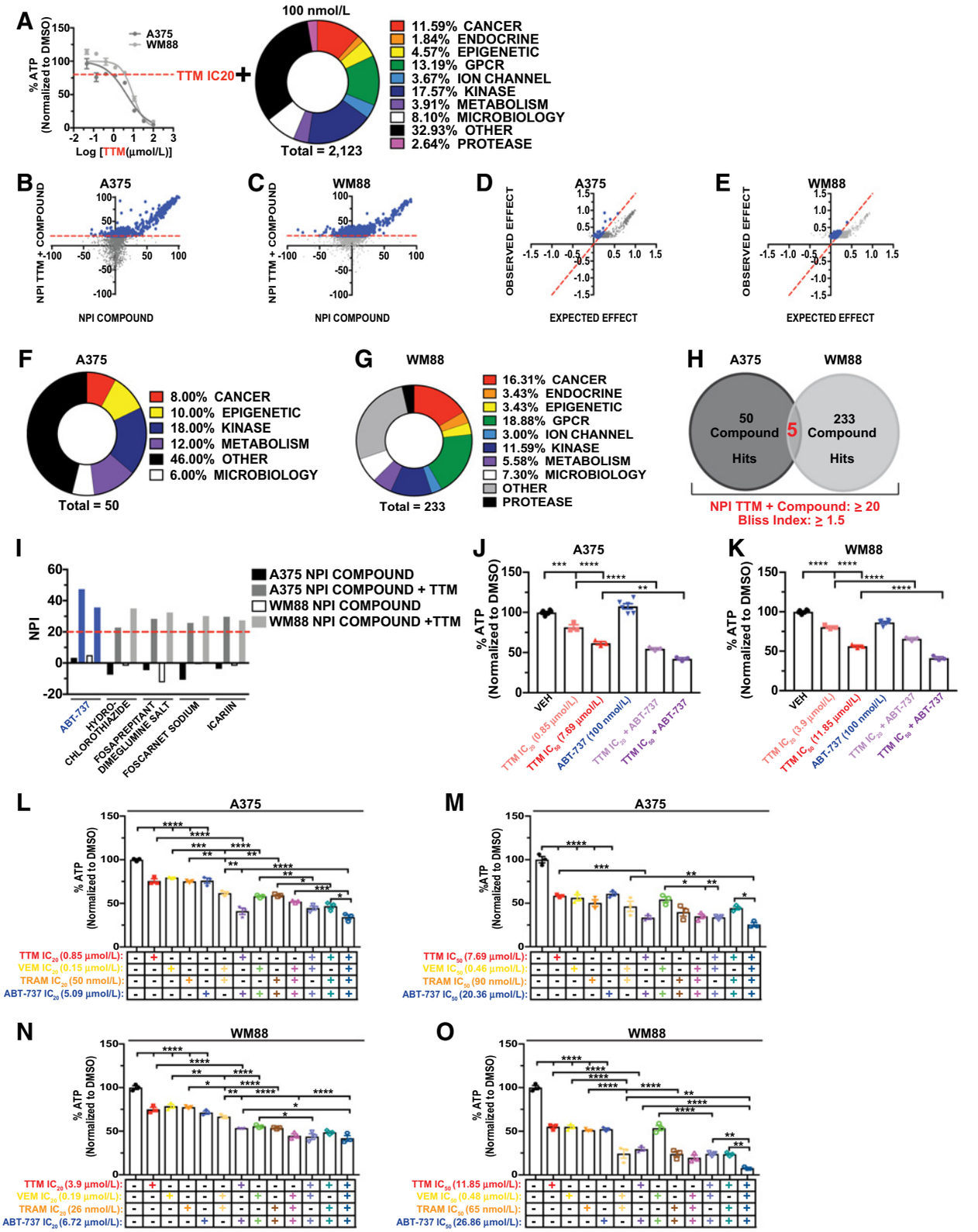

MAPKi-resistant *BRAF* mutation–positive melanoma cells may be driven in part by diminished antiapoptotic protein expression.

To address whether the threshold for apoptosis induction is tipped when MAPKi-resistant BRAF^{V600E}-mutant melanoma cells are treated with the combination of ABT-737 and TTM or a MAPKi, we measured the percentage of apoptotic cells and the levels of markers of apoptosis. Cotreatment with TTM and ABT-737 significantly elevated the number of Annexin V–positive parental and BRAFi-resistant cells, whereas vemurafenib failed to increase the apoptotic response of ABT-737 in the 451-Lu BRAFi^{R} and WM983B BRAFi^{R} cells (**Fig. 6D** and **E**; Supplementary Fig. S7E and S7F). Although the dual combination of trametinib and ABT-737 was sufficient to increase the percentage of apoptotic parental and 451-Lu BRAFi^{R} cells to a similar degree to cotreatment with TTM and ABT-737, apoptotic cell death was only observed in MEK1/2i-resistant 451-Lu cells when TTM and ABT-737 were coadministered (**Fig. 6F**). Further, cotreatment of TTM with ABT-737 was the only combination to result in elevated cleavage of CASPASE-3 and PARP in both the parental and MAPKi-resistant 451-Lu cells (**Fig. 6G–I**; Supplementary Fig. S7G–S7I). These results provide a rationale for a cotreatment strategy with a Cu chelator and BH3 mimetics in the context of MAPKi-resistant forms of BRAF^{V600E} melanoma.

Finally, to extend our findings to *in vitro* models with well-characterized mechanisms of resistance to MAPKi, A375 cells were engineered to stably expressing the p61BRAF^{V600E} splice variant, MEK1^{C121S}, or PDGFRβ (18). As expected, each protein conveyed resistance to vemurafenib, whereas only p61BRAF^{V600E} and MEK1^{C121S} imparted resistance to trametinib (18), as measured by an increase in the IC_{50} of the inhibitors (Supplementary Fig. S8A and S8B). In contrast, TTM reduced the number of viable A375 cells expressing these MAPK-dependent drivers of MAPKi resistance (Supplementary Fig. S8A and S8B). Mechanistically, we previously showed that TTM treatment elicits a reduction in ERK1/2 phosphorylation in A375 cells stably expressing either the p61BRAF^{V600E} splice variant, MEK1^{C121S}, or PDGFRβ (18). TTM was the only compound capable of significantly increasing the cleavage of CASPASE-3 and PARP when combined with ABT-737 in each cell line (Supplementary Fig. S8C and S8D). In summary, these data indicate that MAPK-dependent forms of resistance can be countered by a Cu chelator by mechanistically inhibiting MEK1/2 kinase activity, and apoptosis induction can be achieved when the Cu chelator is combined with BH3 mimetics.

TTM in combination with ABT-263 suppresses growth of naïve and MEK1/2i-resistant BRAF^{V600E}-positive melanoma xenografts

To evaluate the therapeutic potential of combining TTM with BH3 mimetics *in vivo*, we utilized mouse xenograft tumor models of parental and MAPKi-resistant BRAF mutation–positive melanoma. Instead of using ABT-737 for *in vivo* experiments, we evaluated its clinically relevant, orally available analog navitoclax, ABT-263 (36). Mice bearing approximately 100 mm^3 A375 or 451-Lu parental tumors were randomly assigned to one of five treatment arms: (i) vehicle, (ii) TTM, (iii) TTM and ABT-263, (iv) BRAFi, MEK1/2i, and ABT-263, and (v) BRAFi, MEK1/2i, ABT-263, and TTM. These treatments arms were prioritized based on their ability to exam the benefit of combining a Cu chelator and a BH3 mimetic, along with a Cu chelator and the clinically investigated combination of MAPKis and a BH3 mimetic. The growth of established xenograft tumors derived from 451-Lu and A375 cells was reduced when mice were treated with TTM alone and was enhanced when TTM was combined with ABT-263 (**Fig. 7A–F**). Further, growth of the parental tumors was severely reduced when mice were treated for 30 days with the combination of MAPKis and ABT-263, and this reduction in A375 tumor growth was significantly accentuated when TTM was also administered (**Fig. 7A–F**). Although the *in vivo* tumor growth response to the combination of MAPKis and ABT-263 was attenuated in BRAFi-resistant 451-Lu cells, the inclusion of TTM delayed tumor growth and significantly improved the time to endpoint tumor volume (**Fig. 7G–I**). Finally, we demonstrate that xenograft tumors derived from MEK1/2i-resistant 451-Lu cells failed to respond to the combination of MAPKis and ABT-263, but remained sensitive to TTM and ABT-263 dual treatment, which also improved the antitumorigenic properties of the MAPKis (**Fig. 7J–L**). The body weights of mice, monitored as an indicator of drugs toxicity, were similar compared with vehicle group (Supplementary Fig. S9A–S9D). In concordance with reduced tumor growth kinetics, cotreatment with either TTM and ABT-263 or MAPKis and ABT-263 significantly decreased Ki67-positive staining and increased terminal deoxynucleotidyl transferase–mediated dUTP nick end labeling (TUNEL)–positive staining of parental *BRAF*-mutant melanoma tumors (**Fig. 7M–T**; Supplementary Fig. S9E–S9L). Although the addition of TTM to the combination of the MAPKis and ABT-263 did not increase tumor cell apoptosis (**Fig. 7Q–T**; Supplementary Fig. S9I–S9L), cell proliferation was dampened in the parental and MAPKi-resistant tumors (**Fig. 7M–P**; Supplementary Fig. S9E–S9H). As further evidence of apoptosis, cleaved CASPASE-3 and PARP were elevated in parental tumor tissues isolated from mice treated with the dual combination of TTM and ABT-263, the triple combination of MAPKis and ABT-263, and quadruple combination of TTM, MAPKis, and ABT-263 (Supplementary Fig. S9M and S9N). This observation was restricted to the MAPKi-resistant tumors tissue isolated from mice treated with the aforementioned dual and quadruple combinations of TTM and ABT-263 (Supplementary Fig. S9O and S9P). Taken together, these findings support our conclusion that the efficacy of Cu chelators can be enhanced with chemical inducers of apoptosis, and this combination can cooperate with MAPKis to reduce tumor cell growth and survival, especially in the context of refractory or relapsed BRAF^{V600E}-driven melanoma.

Figure 2.

High-throughput screen of bioactive compound library reveals BH3 mimetics as a synergistic combination with TTM in BRAF^{V600E}-positive melanoma cells. **A,** Schematic diagram of high-throughput screen of 2123 Selleckchem bioactive compound library at 100 nmol/L alone or in combination with the IC_{20} of TTM (dashed red line) in A375 or WM88. **B** and **C,** NPI of TTM + Compound versus NPI Compound graph for indicated cells treated with Selleckchem bioactive compound library alone or in combination with IC_{20} of TTM. Hits (blue circles) are defined as NPI TTM + Compound ≥20 (dashed red line). **D** and **E,** Observed effect versus expected effect graph for indicated cells of hits from **B** and **C**. Hits (blue circles) are defined as Bliss Index ≥1.5 (dashed red line). **F** and **G,** Graphical representation of hits defined as NPI TTM + Compound ≥20 and Bliss Index ≥1.5 in indicated cells. **H,** Venn diagram relationship between compound hits. **I,** NPI of 5 overlapping hit compounds from **H** alone or in combination with IC_{20} of TTM (dashed red line). **J** and **K,** Scatter dot plot of %ATP normalized to vehicle ± SEM of indicated cells treated with vehicle or indicated concentrations of drugs. **L–O,** Scatter dot plot of %ATP normalized to vehicle ± SEM of indicated cells treated with vehicle or indicated concentrations of drugs. Results were compared using a one-way ANOVA followed by a Tukey multicomparisons test. *, $P < 0.05$; **, $P < 0.01$; ***, $P < 0.001$; ****, $P < 0.0001$. $n = 3$.

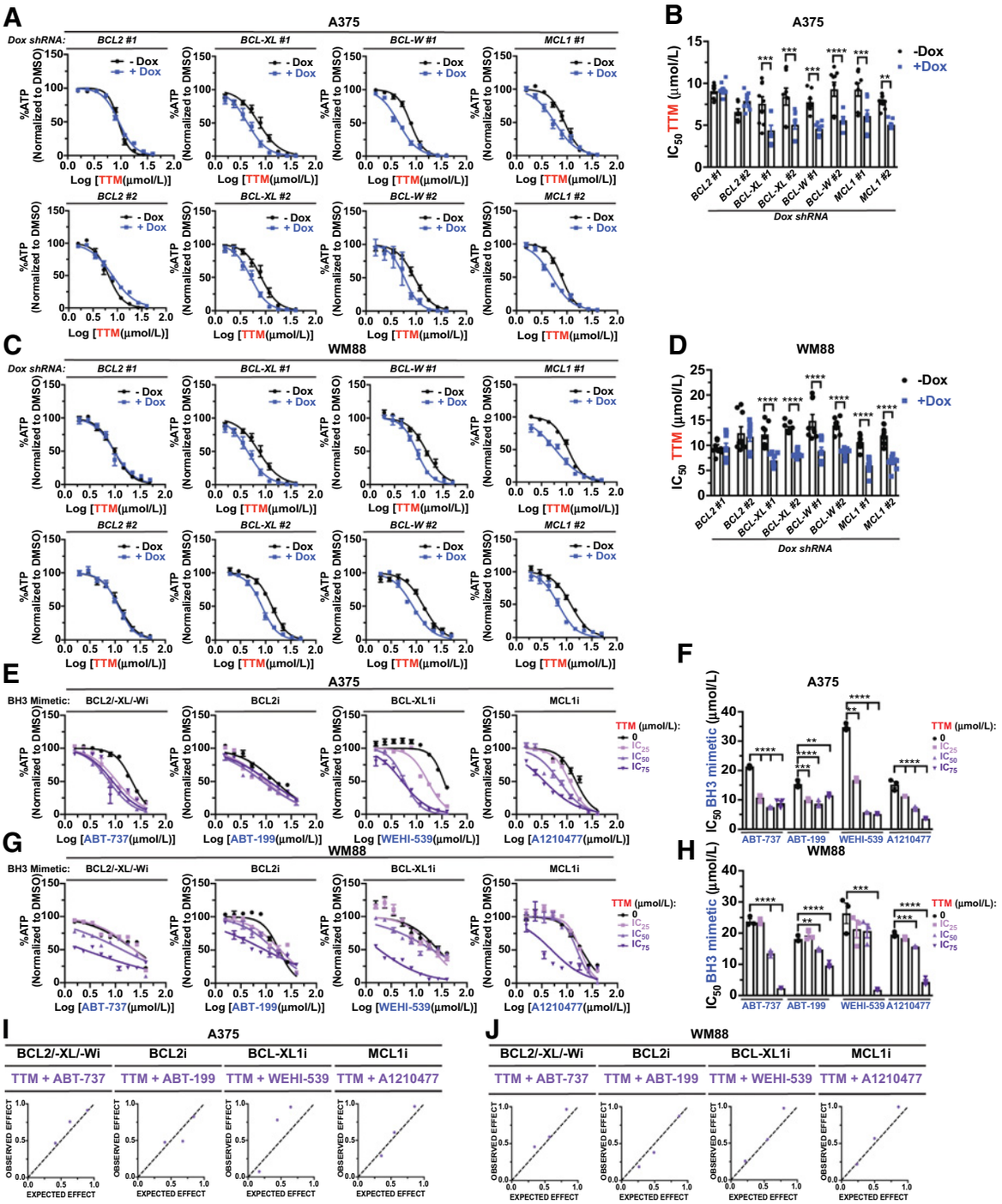

Figure 3.

Targeting select BCL2 family proteins increases sensitivity to TTM in BRAF^{V600E}-positive melanoma. **A** and **C,** Relative CellTiter-Glo cell viability ± SEM of indicated cells stably expressing two independent Dox-inducible *shRNAs* (*#1* and *#2*) against indicated genes treated with indicated concentrations of TTM without or with Dox. $n = 3$. **B** and **D,** Scatter dot plot of TTM IC_{50} ± SEM in indicated cells stably expressing two independent Dox-inducible *shRNAs* against indicated genes treated without or with Dox. Results were compared using a two-way ANOVA followed by a Sidak multicomparisons test. ***, $P < 0.001$; ****, $P < 0.0001$. $n = 3$. **E** and **G,** Relative CellTiter-Glo cell viability ± SEM of indicated cells treated without or with indicated concentrations of TTM and increasing concentrations of indicated BH3 mimetics. $n = 3$. **F** and **H,** Scatter dot plot of BH3 mimetic IC_{50} ± SEM in indicated cells treated without or with indicated concentrations of TTM and increasing concentrations of indicated BH3 mimetics. $n = 3$. Results were compared using a two-way ANOVA followed by a Tukey multicomparisons test. $n = 3$. **I** and **J,** Graphical representation of Bliss Index (observed effect vs. expected effect) from A375 (**E**) and WM88 (**G**) at the indicated drug combinations. Synergistic combinations are indicated by Bliss Index values >1. **, $P < 0.01$; ***, $P < 0.001$; ****, $P < 0.0001$.

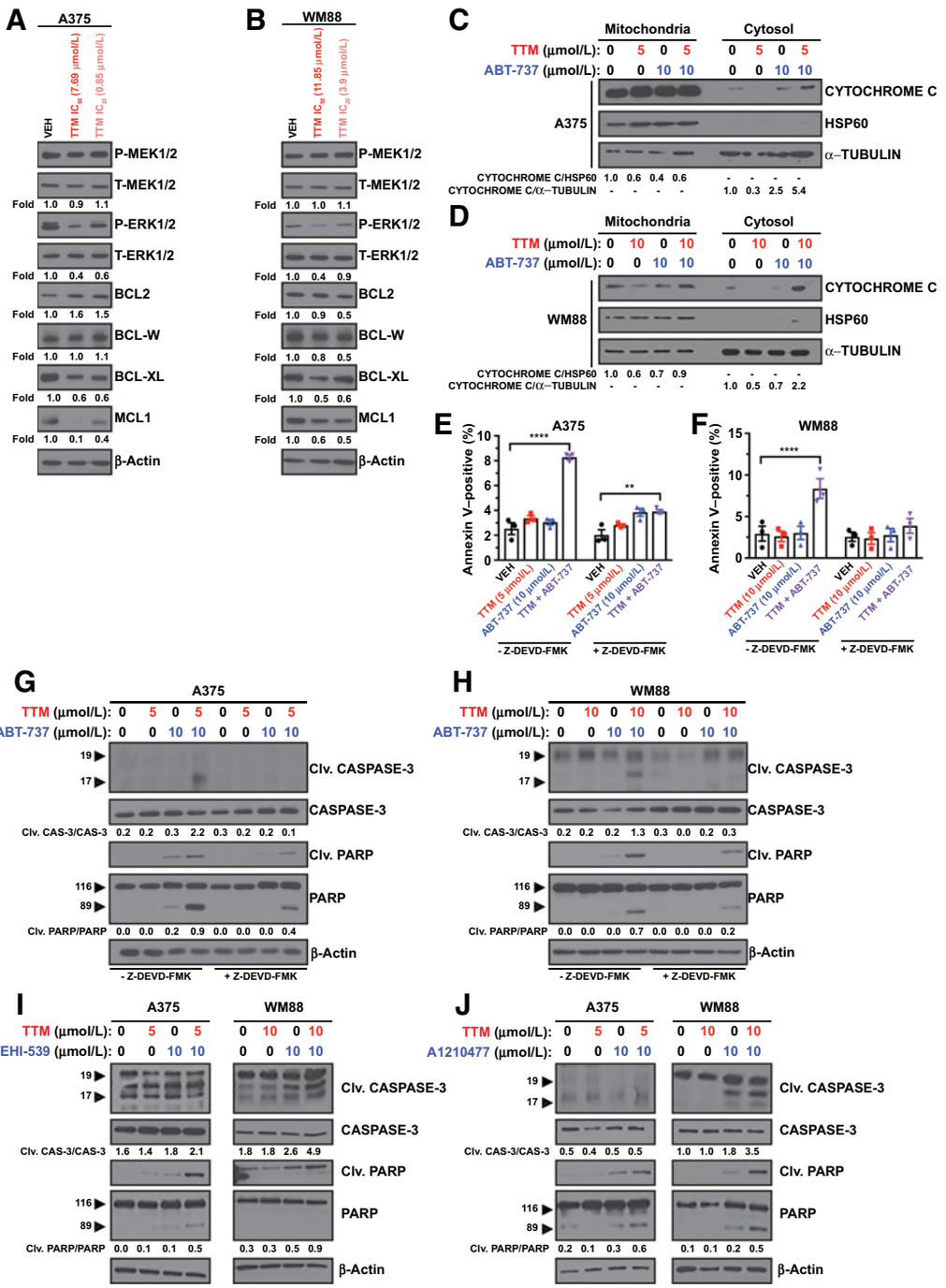

Figure 4.

TTM reduces BCL2 protein expression and lowers the apoptotic threshold when combined with BH3 mimetics in BRAF^{V600E}-positive melanoma. **A** and **B,** Immunoblot detection of phosphorylated (P)-MEK1/2, total (T)-MEK1/2, P-ERK1/2, T-ERK1/2, BCL2, BCL-W, BCL-XL, MCL1, and β-actin from indicated cells treated with vehicle (VEH) or the indicated concentrations of TTM. $n = 3$. **C** and **D,** Immunoblot detection of CYTOCHROME-C, HSP60, and α-TUBULIN of mitochondrial or cytosolic fractions from indicated cells treated with vehicle or the indicated concentrations of drugs. **E** and **F,** Scatter dot plot of flow cytometry analysis of Annexin V-FITC and PI ± SEM stained cells pretreated without or with Z-DEVD-FMK, followed by treatment with vehicle or indicated drugs. $n = 3$. Results were compared using a two-way ANOVA followed by a Tukey multicomparisons test. **, $P < 0.01$; ****, $P < 0.0001$. $n = 3$. **G** and **H,** Immunoblot detection of Cleaved (Clv.) CASPASE-3, CASPASE-3, Clv. PARP, PARP, and β-actin from indicated cells pretreated without or with Z-DEVD-FMK, followed by treatment with vehicle or indicated drugs. **I** and **J,** Immunoblot detection of Clv.CASPASE-3, CASPASE-3, Clv. PARP, PARP, and β-actin from indicated cells treated with vehicle or indicated drugs. Quantification: P-MEK1/2/T-ERK1/2, P-ERK1/2/T-ERK1/2, BCL2 family protein/β-actin, CYTOCHROME-C/HSP60, and CYTOCHROME-C/α-TUBULIN normalized to vehicle control. Fold change Clv. CASPASE-3/CASPASE-3 and Clv. PARP/PARP.

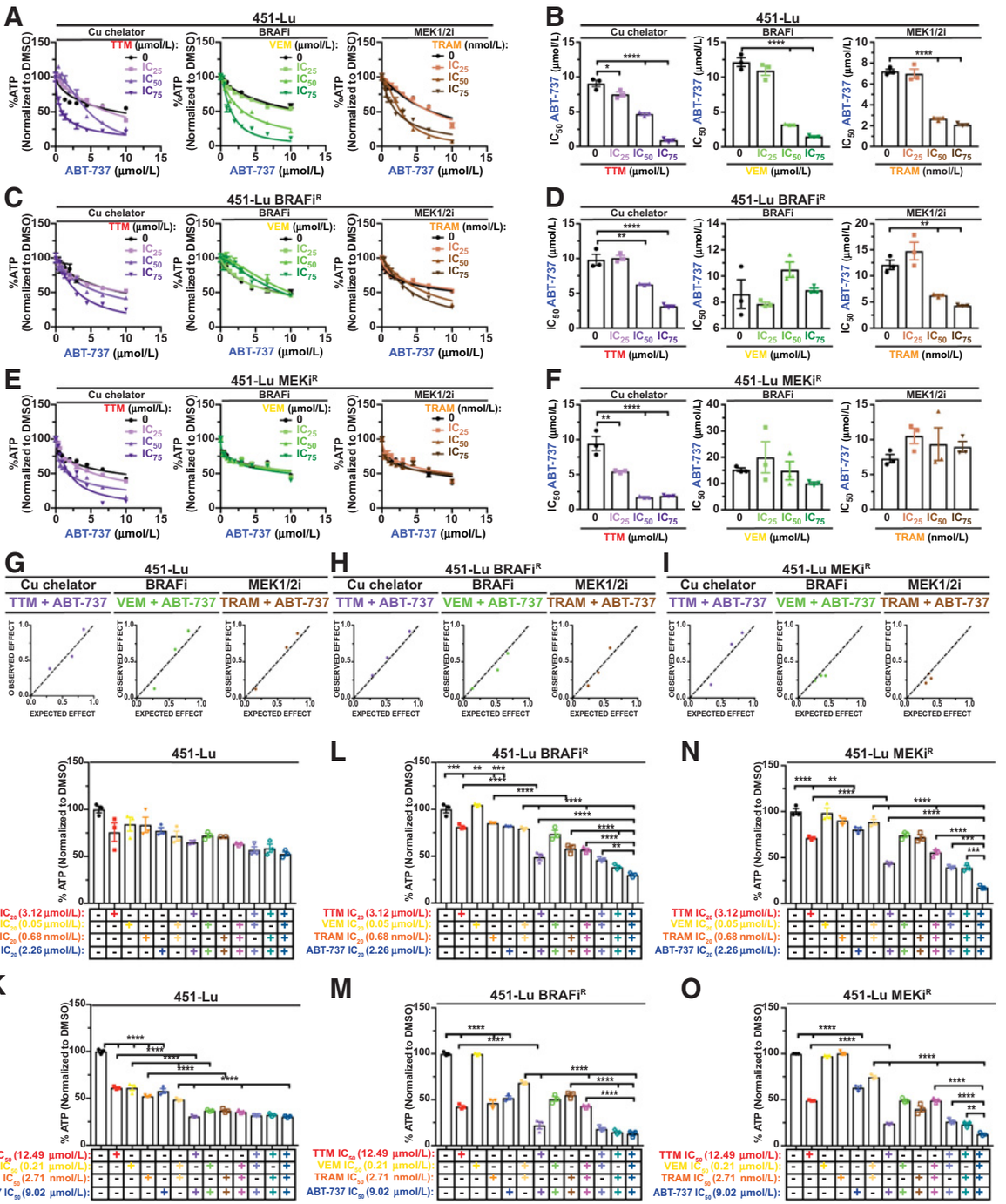

Figure 5.

TTM sensitizes vemurafenib- or trametinib-resistant BRAF^{V600E}-positive melanoma cells to a BCL2 protein inhibitor. **A, C,** and **E,** Relative CellTiter-Glo cell viability ± SEM of indicated cells treated without or with indicated concentrations of TTM, vemurafenib (VEM), or trametinib (TRAM) and increasing concentrations of ABT-737. $n = 3$. **B, D,** and **F,** Scatter dot plot of ABT-737 IC_{50} ± SEM in indicated cells treated without or with indicated concentrations of TTM, vemurafenib, or trametinib and increasing concentrations of ABT-737. $n = 3$. Results were compared using a one-way ANOVA followed by a Dunnett multicomparisons test. $n = 3$. **G–I,** Graphical representation of Bliss Index (observed effect vs. expected effect) from indicated cells at the indicated drug combinations. Synergistic combinations are indicated by Bliss Index values >1. **J–O,** Scatter dot plot of %ATP normalized to vehicle ± SEM of indicated cells treated with vehicle or indicated concentrations of TTM, vemurafenib, trametinib, ABT-737, or the indicated combinations for 72 hours. Results were compared using a one-way ANOVA followed by a Tukey multicomparisons test. $n = 3$. *, $P < 0.05$; **, $P < 0.01$; ***, $P < 0.001$; ****, $P < 0.0001$.

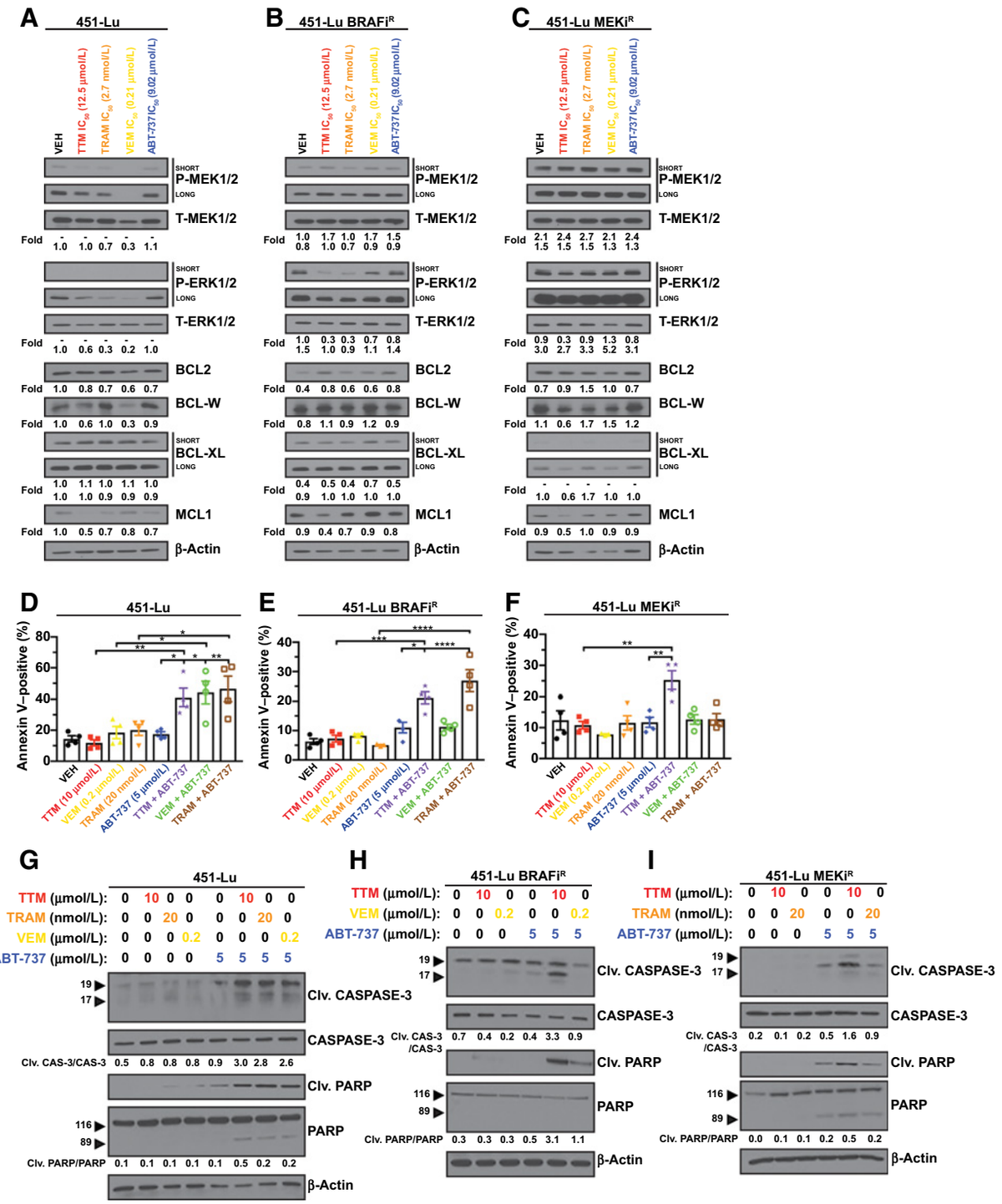

Figure 6.

TTM reduces BCL2 protein expression and lowers the apoptotic threshold when combined with BH3 mimetics in MAPK inhibitor–resistant BRAF^{V600E}-positive melanoma. **A–C,** Immunoblot detection of phosphorylated (P)-MEK1/2, total (T)-MEK1/2, P-ERK1/2, T-ERK1/2, BCL2, BCL-W, BCL-XL, MCL1, and β-actin from indicated cells treated with vehicle (VEH) or the indicated concentrations of TTM, trametinib (TRAM), vemurafenib (VEM), or ABT-737. $n = 3$. **D–F,** Scatter dot plot of flow cytometry analysis of Annexin V-FITC and PI stained ± SEM from indicated cells treated with indicated drugs. $n = 3$. Results were compared using a two-way ANOVA followed by a Tukey multicomparisons test. **, $P < 0.01$; ***, $P < 0.001$; ****, $P < 0.0001$. $n = 3$. **G–I,** Immunoblot detection of Cleaved (Clv.) CASPASE-3, CASPASE-3, Clv. PARP, PARP, and β-actin from indicated cells treated with vehicle, TTM, trametinib, vemurafenib, and/or ABT-737. Quantification: P-MEK1/2/T-ERK1/2, P-ERK1/2/T-ERK1/2, or BCL2 family protein/β-actin, normalized to vehicle control. Fold change Clv. CASPASE-3/CASPASE-3 and Clv. PARP/PARP.

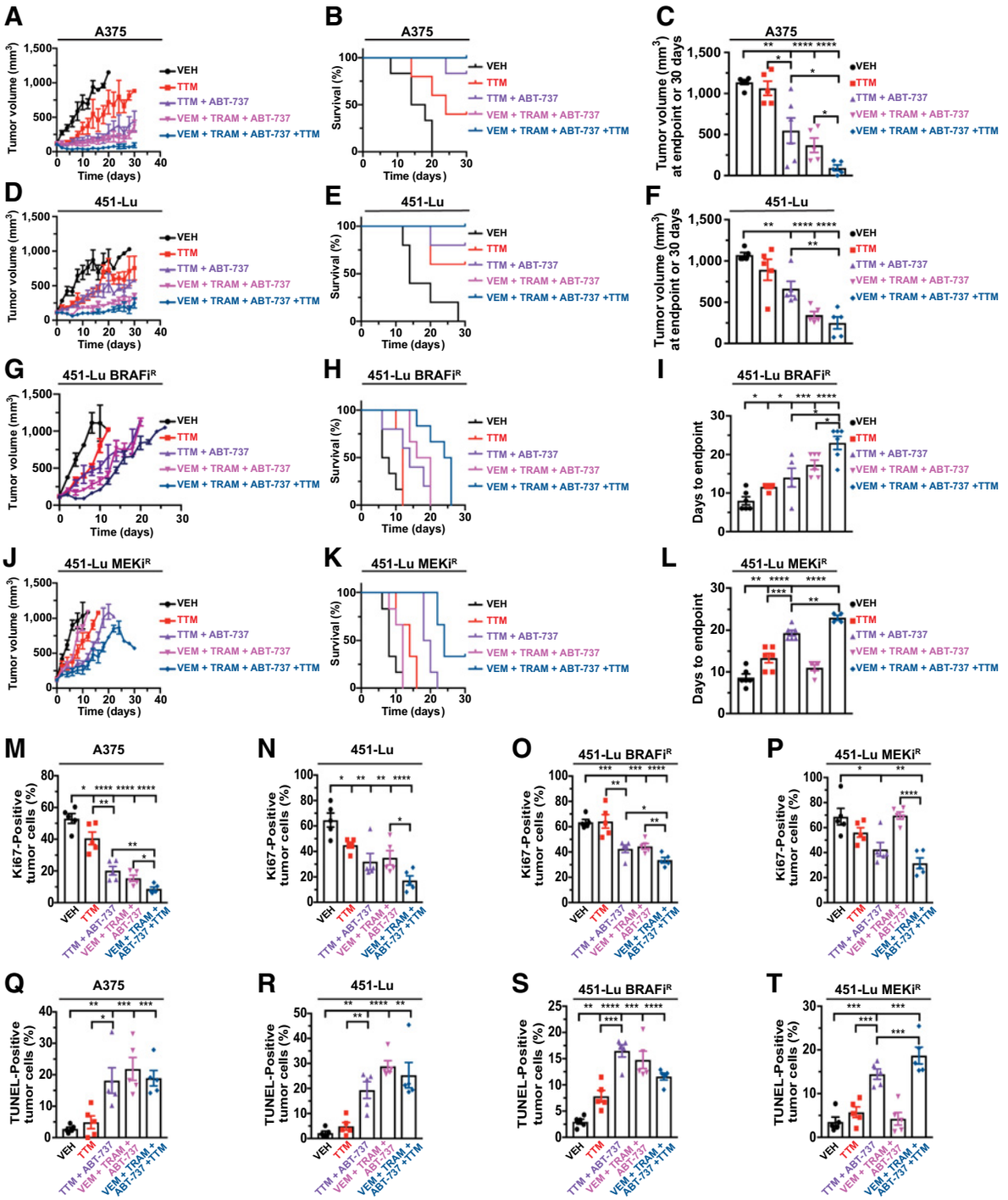

Figure 7.

Cotreatment with TTM and ABT-263 suppresses *in vivo* growth of parental and MAPK inhibitor–resistant $BRAF^{V600E}$-positive melanoma. **A, D, G,** and **J,** Mean tumor volume (mm^3) ± SEM versus time (days) in mice ($n = 5$ or 6) injected with indicated cells and treated with indicated drugs until tumor volume 1.0 cm^3 or for 30 days. **B, E, H,** and **K,** Kaplan–Meier analysis of percentage of mice ($n = 5$ or 6) with tumor volume ≥ 1.0 cm^3 versus time injected with indicated cells treated with indicated drugs. **C** and **F,** Scatter dot plot of tumor volume (mm^3) ± SEM at endpoint of 1.0 cm^3 or at 30 days in mice ($n = 5$ or 6) injected with indicated cells and treated with indicated drugs. Results were compared using unpaired Student *t* test. $n = 5$ or 6. **I** and **L,** Scatter dot plot of days to endpoint tumor volume ± SEM of 1.0 cm^3 or 30 days of mice ($n = 5$ or 6) injected with indicated cells treated with indicated drugs. Results were compared using unpaired Student *t* test. $n = 5$ or 6. **M–T,** Scatter dot plot of % Ki67 or TUNEL-positive cells per tumor ± SEM from mice injected with indicated cells treated with indicated drugs. Results were compared using unpaired Student *t* test. $n = 5$ or 6. *, $P < 0.05$; **, $P < 0.01$; ***, $P < 0.001$; ****, $P < 0.0001$. $n = 5$ or 6.

Discussion

Here, we identified several compounds with the capacity to enhance TTM efficacy in BRAF^{V600E}-driven melanoma, but focused our efforts on an inhibitor of BCL2 antiapoptotic proteins. Although the combination of ABT-737 and a BRAFi induces apoptosis in BRAF^{V600E}-mutant melanoma cells (52–54), it is not effective in BRAFi-resistant cells and required additional targeted or conventional chemotherapeutics to tip the apoptotic threshold toward cell death (54). The absence of efficacy achieved with ABT-737 and BRAFi in the context of resistance may be driven by a unique repertoire of BCL2 proteins in melanocytes (45, 46, 49–51, 54, 56). In addition, proapoptotic BH3-only proteins' expression patterns or their different binding affinity to the antiapoptotic proteins can induce different dependencies on BCL2 proteins (34, 45, 57). Recently, Lee and colleagues defined that BCL-XL and MCL1 dual targeting is critical to blunt melanoma cell survival, but it remains to be determined whether their combination targeting would reduce MAPKi-resistant melanoma cell viability (58).

Mechanistically, genetic knockdown of *BCL-XL, BCL-W*, or *MCL1*, but not BCL2, revealed that several BCL2 proteins were involved in the synergistic reduction in cell viability and induction of apoptotic cell death elicited by cotargeting the MAPK pathway with TTM and antiapoptotic machinery with BH3 mimetics (**Figs. 3** and **4**; Supplementary Figs. S4 and S6). Mechanistically, the Cu chelator lowered the threshold for apoptotic cell death by limiting the expression of several BCL2 proteins (**Fig. 4**; Supplementary Fig. S7). Encouragingly, BRAF^{V600E}-mutant melanoma tumor growth was effectively suppressed and controlled when TTM was combined with ABT-263 without negatively affecting animal welfare, suggesting that Cu chelation could be added to current efforts to evaluate MAPKi with navitoclax in *BRAF* mutation–positive melanoma (NCT01989585; **Fig. 7**; Supplementary Fig S9). Our results provide the possibility that BH3 mimetics can be an effective therapeutic with less adverse effects when dosed with a Cu chelator based on the synergistic combination, which is not achieved with vemurafenib or trametinib (**Figs. 3** and **5**; Supplementary Fig. S5). Finally, in the setting of MAPKi-resistant BRAF^{V600E}-driven melanoma, TTM in combination with ABT-737 *in vitro* or ABT-263 *in vivo* reduced cell viability, decreased tumor growth kinetics, reduced tumor proliferation, and triggered apoptotic cell death (**Figs. 5–7**; Supplementary Figs. S6–S9). These findings highlight a need for additional exploration of the interplay between Cu-dependent MAPK signaling and cellular intrinsic apoptotic pathways. Thus, we provide a proof of concept that Cu chelation therapy synergistically improves BH3 mimetic efficacy by inducing apoptosis and supports the utility of this combination in patients with *BRAF* mutation–positive melanoma that do not respond to targeted therapy or immunotherapy, have severe side effects, or acquire resistance.

Disclosure of Potential Conflicts of Interest

D.C. Brady has an ownership interest (including patents) in Merlon Inc. No potential conflicts of interest were disclosed by the other authors.

Authors' Contributions

Conception and design: Y.-J. Kim, D.C. Brady
Development of methodology: Y.-J. Kim, T. Tsang, D.C. Brady
Acquisition of data (provided animals, acquired and managed patients, provided facilities, etc.): Y.-J. Kim, J.M. Posimo
Analysis and interpretation of data (e.g., statistical analysis, biostatistics, computational analysis): Y.-J. Kim, T. Tsang, G.R. Anderson, D.C. Brady
Writing, review, and/or revision of the manuscript: Y.-J. Kim, T. Tsang, G.R. Anderson, J.M. Posimo, D.C. Brady
Administrative, technical, or material support (i.e., reporting or organizing data, constructing databases): Y.-J. Kim, D.C. Brady
Study supervision: D.C. Brady

Acknowledgments

We thank J. Villanueva (The Wistar Institute) for cell lines, S. Cherry and D.C. Schultz of the University of Pennsylvania High-Throughput Screening Core for technical support, I.A. Asangani, L. Busino, T.P. Gade, B.J. Kim, S.W. Ryeom, and E.S. Witze (University of Pennsylvania) for technical support, discussions, and/or review of the article, and D. Sneddon for administrative support. This work was supported by the Pew Charitable Trust Pew Scholars Program in Biomedical Science Award #50359 (D.C. Brady) and by a pilot project from Tara Miller Foundation at University of Pennsylvania/Wistar Institute supported by Skin Cancer SPORE Career Enhancement Program Award to D.C. Brady (P50CA174523). T. Tsang is supported by NCI NRSA Fellowship (F31) F31CA243294. G.R. Anderson is supported by NCI Predoctoral to Postdoctoral Transition Fellowship (F99/K00) K00CA222728. J.M. Posimo is supported by American Cancer Society Postdoctoral Fellowship 131203PF1714701CCG. This work is dedicated in the memory of Maria Whitehead.

The costs of publication of this article were defrayed in part by the payment of page charges. This article must therefore be hereby marked *advertisement* in accordance with 18 U.S.C. Section 1734 solely to indicate this fact.

Received June 6, 2019; revised December 17, 2019; accepted January 27, 2020; published first January 31, 2020.

References

1. Davies H, Bignell GR, Cox C, Stephens P, Edkins S, Clegg S, et al. Mutations of the BRAF gene in human cancer. Nature 2002;417:949–54.
2. Siegel RL, Miller KD, Jemal A. Cancer statistics, 2019. CA Cancer J Clin 2019; 7–34.
3. The Cancer Genome Atlas Network. Genomic classification of cutaneous melanoma. Cell 2015;161:1681–96.
4. Holderfield M, Deuker MM, McCormick F, McMahon M. Targeting RAF kinases for cancer therapy: BRAF-mutated melanoma and beyond. Nat Rev Cancer 2014;14:455–67.
5. Wan PTC, Garnett MJ, Roe SM, Lee S, Niculescu-Duvaz D, Good VM, et al. Mechanism of activation of the RAF-ERK signaling pathway by oncogenic mutations of B-RAF. Cell 2004;116:855–67.
6. Flaherty KT, Infante JR, Daud A, Gonzalez R, Kefford RF, Sosman J, et al. Combined BRAF and MEK inhibition in melanoma with BRAF V600 mutations. N Engl J Med 2012;367:1694–703.
7. Robert C, Karaszewska B, Schachter J, Rutkowski P, Mackiewicz A, Stroiakovski D, et al. Improved overall survival in melanoma with combined dabrafenib and trametinib. N Engl J Med 2015;372:30–9.
8. Larkin J, Ascierto PA, Dreno B, Atkinson V, Liszkay G, Maio M, et al. Combined vemurafenib and cobimetinib in BRAF-mutated melanoma. N Engl J Med 2014; 371:1867–76.
9. Long G V., Stroyakovskiy D, Gogas H, Levchenko E, De Braud F, Larkin J, et al. Dabrafenib and trametinib versus dabrafenib and placebo for Val600 BRAF-mutant melanoma: a multicentre, double-blind, phase 3 randomised controlled trial. Lancet 2015;386:444–51.
10. Caunt CJ, Sale MJ, Smith PD, Cook SJ. MEK1 and MEK2 inhibitors and cancer therapy: the long and winding road. Nat Rev Cancer 2015; 15:577–92.
11. Solit DB, Rosen N. Towards a unified model of RAF inhibitor resistance. Cancer Discov 2014;4:27–30.
12. Friedman A, Perrimon N. High-throughput approaches to dissecting MAPK signaling pathways. Methods 2006;40:262–71.
13. Friedman A, Perrimon N. A functional RNAi screen for regulators of receptor tyrosine kinase and ERK signalling. Nature 2006;444:230–4.
14. Turski ML, Brady DC, Kim HJ, Kim B-E, Nose Y, Counter CM, et al. A novel role for copper in Ras/MAPK signaling. Mol Cell Biol 2012;32:1284–95.

15. Solit DB, Garraway LA, Pratilas CA, Sawai A, Getz G, Basso A, et al. BRAF mutation predicts sensitivity to MEK inhibition. Nature 2006;439:358–62.
16. Brady DC, Crowe MS, Turski ML, Hobbs GA, Yao X, Chaikuad A, et al. Copper is required for oncogenic BRAF signalling and tumorigenesis. Nature 2014;509: 492–6.
17. Brewer GJ, Askari F, Lorincz MT, Carlson M, Schilsky M, Kluin KJ, et al. Treatment of wilson disease with ammonium tetrathiomolybdate. Arch Neurol 2006;63:521–7.
18. Brady DC, Crowe MS, Greenberg DN, Counter CM. Copper chelation inhibits BRAFV600E-driven melanomagenesis and counters resistance to BRAFV600E and MEK1/2 inhibitors. Cancer Res 2017;77:6240–52.
19. Chan N, Willis A, Kornhauser N, Mward M, Lee SB, Nackos E, et al. Influencing the tumor microenvironment: a phase II study of copper depletion using tetrathiomolybdate in patients with breast cancer at high risk for recurrence and in preclinical models of lung metastases. Clin Cancer Res 2017;23:666–76.
20. Villanueva J, Vultur A, Lee JT, Somasundaram R, Fukunaga-Kalabis M, Cipolla AK, et al. Acquired resistance to BRAF inhibitors mediated by a RAF kinase switch in melanoma can be overcome by cotargeting MEK and IGF-1R/PI3K. Cancer Cell 2010;18:683–95.
21. Villanueva J, Infante JR, Krepler C, Reyes-Uribe P, Samanta M, Chen HY, et al. Concurrent MEK2 mutation and BRAF amplification confer resistance to BRAF and MEK inhibitors in melanoma. Cell Rep 2013;4:1090–9.
22. Foucquier J, Guedj M. Analysis of drug combinations: current methodological landscape. Pharmacol Res Perspect 2015;3:e00149.
23. Hamad NM, Elconin JH, Karnoub AE, Bai W, Rich JN, Abraham RT, et al. Distinct requirements for Ras oncogenesis in human versus mouse cells. Genes Dev 2002;16:2045–57.
24. Vermes I, Haanen C, Steffens-Nakken H, Reutelingsperger C. A novel assay for apoptosis. Flow cytometric detection of phosphatidylserine expression on early apoptotic cells using fluorescein labelled annexin V. J Immunol Methods 1995; 184:39–51.
25. Nicholson DW, Ali A, Thornberry NA, Vaillancourt JP, Ding CK, Gallant M, et al. Identification and inhibition of the ICE/CED-3 protease necessary for mammalian apoptosis. Nature 1995;376:37–43.
26. Li P, Nijhawan D, Budihardjo I, Srinivasula SM, Ahmad M, Alnemri ES, et al. Cytochrome c and dATP-dependent formation of Apaf-1/caspase-9 complex initiates an apoptotic protease cascade. Cell 1997;91:479–89.
27. Chipuk JE, Moldoveanu T, Llambi F, Parsons MJ, Green DR. The BCL-2 family reunion. Mol Cell 2010;37:299–310.
28. Boise LH, González-García M, Postema CE, Ding L, Lindsten T, Turka LA, et al. bcl-x, a bcl-2-related gene that functions as a dominant regulator of apoptotic cell death. Cell 1993;74:597–608.
29. Gibson L, Holmgreen SP, Huang DC, Bernard O, Copeland NG, Jenkins NA, et al. bcl-w, a novel member of the bcl-2 family, promotes cell survival. Oncogene 1996;13:665–75.
30. Kozopas KM, Yang T, Buchan HL, Zhou P, Craig RW. MCL1, a gene expressed in programmed myeloid cell differentiation, has sequence similarity to BCL2. Proc Natl Acad Sci U S A 1993;90:3516–20.
31. Oltvai ZN, Milliman CL, Korsmeyer SJ. Bcl-2 heterodimerizes in vivo with a conserved homolog, Bax, that accelerates programmed cell death. Cell 1993;74: 609–19.
32. Chittenden T, Flemington C, Houghton AB, Ebb RG, Gallo GJ, Elangovan B, et al. A conserved domain in Bak, distinct from BH1 and BH2, mediates cell death and protein binding functions. EMBO J 1995;14:5589–96.
33. O'Connor L, Strasser A, O'Reilly LA, Hausmann G, Adams JM, Cory S, et al. Bim: a novel member of the Bcl-2 family that promotes apoptosis. EMBO J 1998;17: 384–95.
34. Letai AG. Diagnosing and exploiting cancer's addiction to blocks in apoptosis. Nat Rev Cancer 2008;8:121–32.
35. Delbridge ARD, Strasser A. The BCL-2 protein family, BH3-mimetics and cancer therapy. Cell Death Differ 2015;22:1071–80.
36. Tse C, Shoemaker AR, Adickes J, Anderson MG, Chen J, Jin S, et al. ABT-263: a potent and orally bioavailable Bcl-2 family inhibitor. Cancer Res 2008;68:3421–8.
37. Oltersdorf T, Elmore SW, Shoemaker AR, Armstrong RC, Augeri DJ, Belli BA, et al. An inhibitor of Bcl-2 family proteins induces regression of solid tumours. Nature 2005;435:677–81.
38. Souers AJ, Leverson JD, Boghaert ER, Ackler SL, Catron ND, Chen J, et al. ABT-199, a potent and selective BCL-2 inhibitor, achieves antitumor activity while sparing platelets. Nat Med 2013;19:202–8.
39. Lessene G, Czabotar PE, Sleebs BE, Zobel K, Lowes KN, Adams JM, et al. Structure-guided design of a selective BCL-XL inhibitor. Nat Chem Biol 2013;9: 390–7.
40. Leverson JD, Zhang H, Chen J, Tahir SK, Phillips DC, Xue J, et al. Potent and selective small-molecule MCL-1 inhibitors demonstrate on-target cancer cell killing activity as single agents and in combination with ABT-263 (navitoclax). Cell Death Dis 2015;6:e1590.
41. Davids MS, Seymour JF, Gerecitano JF, Kahl BS, Pagel JM, Wierda WG, et al. Phase I study of ABT-199 (GDC-0199) in patients with relapsed/refractory (R/R) non-Hodgkin lymphoma (NHL): responses observed in diffuse large B-cell (DLBCL) and follicular lymphoma (FL) at higher cohort doses. J Clin Oncol 2017;32:8522.
42. Konopleva M, Pollyea DA, Potluri J, Chyla B, Hogdal L, Busman T, et al. Efficacy and biological correlates of response in a phase II study of venetoclax monotherapy in patients with acute myelogenous leukemia. Cancer Discov 2016;6: 1106–17.
43. Vogler M, Dinsdale D, Dyer MJS, Cohen GM. ABT199 selectively inhibits BCL2 but not BCL2L1 and efficiently induces apoptosis of chronic lymphocytic leukaemic cells but not platelets. Br J Haematol 2013;163:139–42.
44. Seymour JF, Davids MS, Pagel JM, Kahl BS, Wierda WG, Miller TP, et al. Bcl-2 inhibitor ABT-199 (GDC-0199) monotherapy shows anti-tumor activity including complete remissions in high-risk relapsed/refractory (R/R) chronic lymphocytic leukemia (CLL) and small lymphocytic lymphoma (SLL). Blood 2013; 122:872.
45. Soderquist RS, Crawford L, Liu E, Lu M, Agarwal A, Anderson GR, et al. Systematic mapping of BCL-2 gene dependencies in cancer reveals molecular determinants of BH3 mimetic sensitivity. Nat Commun 2018;9:3513.
46. Anvekar RA, Asciolla JJ, Missert DJ, Chipuk JE. Born to be alive: a role for the BCL-2 family in melanoma tumor cell survival, apoptosis, and treatment. Front Oncol 2011;1.
47. Gautschi O, Tschopp S, Olie RA, Leech SH, Simões-Wüst AP, Ziegler A, et al. Activity of a novel bcl-2/bcl-xL-bispecific antisense oligonucleotide against tumors of diverse histologic origins. J Natl Cancer Inst 2001;93:463–71.
48. Del Bufalo D, Trisciuoglio D, Scarsella M, Zangemeister-Wittke U, Zupi G. Treatment of melanoma cells with a bcl-2/bcl-xL antisense oligonucleotide induces antiangiogenic activity. Oncogene 2003;22:8441–7.
49. Thallinger C, Wolschek MF, Wacheck V, Maierhofer H, Gunsberg P, Polterauer P, et al. Mcl-1 antisense therapy chemosensitizes human melanoma in a SCID mouse xenotransplantation model. J Invest Dermatol 2003;120:1081–6.
50. Keuling AM, Felton KEA, Parker AAM, Akbari M, Andrew SE, Tron VA. RNA silencing of Mcl-1 enhances ABT-737-mediated apoptosis in melanoma: role for a caspase-8-dependent pathway. PLoS One 2009;4:e6651.
51. Nguyen M, Marcellus RC, Roulston A, Watson M, Serfass L, Madiraju SRM, et al. Small molecule obatoclax (GX15-070) antagonizes MCL-1 and overcomes MCL-1-mediated resistance to apoptosis. Proc Natl Acad Sci U S A 2007;104:19512–7.
52. Cragg MS, Jansen ES, Cook M, Harris C, Strasser A, Scott CL. Treatment of B-RAF mutant human tumor cells with a MEK inhibitor requires Bim and is enhanced by a BH3 mimetic. J Clin Invest 2008;118:3651–9.
53. Serasinghe MN, Missert DJ, Asciolla JJ, Podgrabinska S, Wieder SY, Izadmehr S, et al. Anti-apoptotic BCL-2 proteins govern cellular outcome following B-RAF (V600E) inhibition and can be targeted to reduce resistance. Oncogene 2015;34: 857–67.
54. Wroblewski D, Mijatov B, Mohana-Kumaran N, Lai F, Gallagher SJ, Haass NK, et al. The BH3-mimetic ABT-737 sensitizes human melanoma cells to apoptosis induced by selective BRAF inhibitors but does not reverse acquired resistance. Carcinogenesis 2013;34:237–47.
55. McGill GG, Horstmann M, Widlund HR, Du J, Motyckova G, Nishimura EK, et al. Bcl2 regulation by the melanocyte master regulator Mitf modulates lineage survival and melanoma cell viability. Cell 2002;109:707–18.
56. Tang L, Tron VA, Reed JC, Mah KJ, Krajewska M, Li G, et al. Expression of apoptosis regulators in cutaneous malignant melanoma. Clin Cancer Res 1998;4: 1865–71.
57. Certo M, Del Gaizo Moore V, Nishino M, Wei G, Korsmeyer S, Armstrong SA, et al. Mitochondria primed by death signals determine cellular addiction to antiapoptotic BCL-2 family members. Cancer Cell 2006;9:351–65.
58. Lee EF, Harris TJ, Tran S, Evangelista M, Arulananda S, John T, et al. BCL-XL and MCL-1 are the key BCL-2 family proteins in melanoma cell survival. Cell Death Dis 2019;10:342.